Journal of Applied Fluid Mechanics, Vol. 16, No. 9, pp. 1806-1817, 2023.
Available online at www.jafmonline.net, ISSN 1735-3572, EISSN 1735-3645.
https://doi.org/10.47176/jafm.16.09.1828

Numerical Simulation of Hatchback Car with Modified Vehicle Design for the Improvement of Fuel Consumption

G. Sivaraj[1†], K. M. Parammasivam[2], M. S. Prasath[1] and D. Lakshmanan[1]

[1] *Subsonic Airflow Testing Facility, Research Park, Bannari Amman Institute of Technology, Tamilnadu, India – 638401*
[2] *Department of Aerospace Engineering, Anna University (MIT Campus), Chennai, India – 600044*

†*Corresponding Author Email: sivarajg@bitsathy.ac.in*

ABSTRACT

The continuous demand and fuel depletion in the automobile industries cause a reduction in fuel consumption, especially in a car which is a classic problem to focus on vehicle body design. The formation of drag force in the car body demands tractive force and significantly affects the engine performance and fuel consumption rate which is not advisable for enhancing aerodynamic efficiency. This paper discusses the methodology to reduce the fuel consumption rate in hatchback cars using a 'basebleed method'. The hatchback car model with and without basebleed is numerically simulated for the various speed to study the aerodynamic coefficients. The numerical simulation is performed with the *k-ε* turbulence model for predicting the wake region of both car models with and without basebleed. The numerical study witnessed the hatchback car model with basebleed arrived 6% reduction in the coefficient of drag (C_D) compared to without basebleed, which results in a reduction of fuel consumption rate of up to 4.33 %. The research evidence that the stability of the car is not affected while using this basebleed drag reduction method and it is studied from the resultant parameters such as coefficient of lift (C_L) and coefficient of side force (C_S) and for the varying yaw angle (φ). Further, the research recommends the integration of basebleed at the underbody structure in Hatchback cars to improve the engine fuel consumption without affecting its stability.

Article History

Received February 20, 2023
Revised April 24, 2023
Accepted April 25, 2023
Available online July 1, 2023

Keywords:

Hatchback car
Vehicle design
CFD
Drag force
Fuel consumption

1. INTRODUCTION

The world economy is widely affected by the hike in fuel prices in recent years. The impact of fluctuation in worldwide oil prices is often reflected in the Automobile sector. Hence, a small step toward a reduction in fuel consumption will be an extraordinary accomplishment in the field of automobiles. Automobile design is one such field where airflow behaviour has its application to designing a most streamlined vehicle to draw an efficient vehicle performance with reduced drag. The drag created by the vehicle due to its shape is directly related to the power and hence the fuel consumption. Hence, automobile aerodynamics design – a field of investigation of airflow and, forces and moments acting on the body of an automobile, gained attention during the early 20th century. It resulted in an ample amount of research studies focusing on automobile aerodynamics design, both internally and externally, and aerodynamics-based design optimization of automobiles (Rakibul et al., 2014). As a result of design evolution, the co-efficient of drag (C_D) – a non-dimensional parameter representing drag, has reduced from 0.5 to 0.3 for a wide range of automobiles (Hucho & Sovran, 1993), whereas some automobile industries still produce cars with C_D of 0.45 (Ex: Jeep Wrangler (JL) produced in 2018).

Since some researchers have been concentrating on the reduction of drag in vehicles for better fuel consumption and comfortable riding. At present, drag reduction is achieved either by shape optimization or by incorporating drag reduction devices that also lead to higher stability of the car (Siddiqui & Chaab, 2021). Aerodynamic drag reduction devices such as vortex generators, diffusers, front spoilers, rear spoilers, splitters, and guide vanes, etc. research is being conducted all over the world as well as Matthew & Simon (2014) investigated the wake regions of the aerodynamic structure of Formula 1 Car. This work addressed the wake region and its impact on airflow on the far field from the vehicle. The raised ground plane technique was practically utilized to examine the far-field flow dynamics. The study reported the formation of more turbulent regions due to merging the low-speed stream from the diffuser with counter-rotating vortices.

Nomenclature

A_f	frontal area	f_y	body force in y direction
B_f	the distance between the basebleed inlets at the front end	f_z	body force in z direction
B_r	the distance between the basebleed at the rear end	H_f	the height of the basebleed at the front end
C_D	co-efficient of Drag	H_r	the height of the basebleed at the rear end
C_L	co-efficient of Lift	L	lift force
C_P	co-efficient of Pressure	S	side force
C_S	co-efficient of Side force	U	vehicle speed
D	drag force	φ	slant angle
FC	fuel consumption	ψ	yaw angle
f_x	body force in x direction		

Gregoire et al. (2011) conducted experimental studies on a bluff body with a deflector for drag reduction. The deflector was installed in the model at the top of the rear window to remove the wake region around the rear side. The drag force was reduced up to 9% by adding a deflector on the model. The Wake analyses show that the deflector improves the streamlined flow around the bluff body. Kang et al. (2012) carried out research to develop various types of diffusers for the reduction of drag on sedan cars.

They designed round and arc-shaped diffusers to create a streamline flow under the body and mounted them on the rear side. The rear side pressure is rising due to the reduction of the wake region by attaching a diffuser which restricts the recirculation of air coming under the body to the rear side of the car. The vehicle drag was diminished by 4%, which improves the fuel efficiency by roughly 2% when the speed of the vehicle exceeds 19 m/s.

The researchers began researching concentrate on reducing the wake region at the rear side of the vehicle and maintaining the streamline around the vehicle. Mahmoud et al. (2012). focused on the aerodynamic design of the vehicle to enhance the vehicle performance by reducing drag and lift. Experiments were performed on a simplified car with an attachment of a flexible air inlet and different types of air outlets. Charalampos et al. (2016) investigated the rear-end flow structure of a sedan car. They focused on improving the flow region at the car's rear side to get better drag reduction. Experimental and computational studies were done with two car models – a 1:4 scaled Volvo s60 and a full-scale model of a 2010MY vehicle. Renan and Francisco (2015) conducted a computational analysis of a fastback car for the reduction of drag at high-speed using suction and blowing jets toward the rear side of the car. While the vehicle is moving at high speed, the airflow goes through the jets and injects the flow towards the rear side wake region thus reducing the drag force. The authors have done another consecutive work of analyzing the same phenomenon in a three-dimensional car. Wake formation and turbulent kinetic energy were analyzed in that study.

Andrew et al. (2009) have reduced the drag on bluff two-box SUVs using basebleed. This research significantly reduces the drag force for increasing the mass flow rate of air at the rear side of the region by outlet on the upper and side sections of the vehicle. Marklund et al. (2013) reported the aerodynamic performance of a sedan car model and a square back car model installed with a smooth underbody diffuser at the rear end of the car. The studies were done with and without covering the underbody. The aerodynamic underbody diffuser with an underbody cover reduced the C_D value by 0.035 from the base vehicle, but without covering the underbody the coefficient of drag (C_D) value increased by 0.006 from the base vehicle. The same study was repeated for wagon vehicles equipped with underbody diffusers using experimental and computational methods and observed the drag reduction ranges of 3%.

Since hatchback cars provide sufficient comfort in an affordable price range, people from lower- and middle-income countries like India prefer those cars. However, the drag generated by this type of car is significant enough to affect fuel consumption and burden the economy. Though the drag reduction devices are found to reduce overall drag force to an extent, the penalty on stability and related engine performance doesn't contribute much to the overall vehicle performance (Yang et al., 2022). This restricts the usage of such drag-reduction devices in passenger cars. Most of the researchers concentrate only on reducing the drag and lift coefficient but neglect to analyze the effect of stability on the vehicle. Hence, it is highly essential to design a drag reduction technique for hatchback cars without affecting stability so that the vehicle performance can be improved.

Based on such a necessity, the objectives of the present study are to numerically evaluate the drag reduction performance of the chosen configuration compared with a base model and evaluate the side force effects for stability analysis. In order to meet the above objectives a drag reduction technique - "basebleed method" was introduced in this study. The wake profiles of hatchback car with and without basebleed is carried out with the help of streamline pattern in the numerical simulation. The coefficient of pressure C_L distribution of the base model and with and without basebleed technique is compared. Further, the velocity and turbulent intensity are also obtained for the models with and without the basebleed in the hatchback car model. A negligible effect of the basebleed technique on C_L and C_S is observed for stability analysis.

1.1 Flow Processes

The flow field of a car is contributed by airflow over and inside the car, and airflow is produced by the

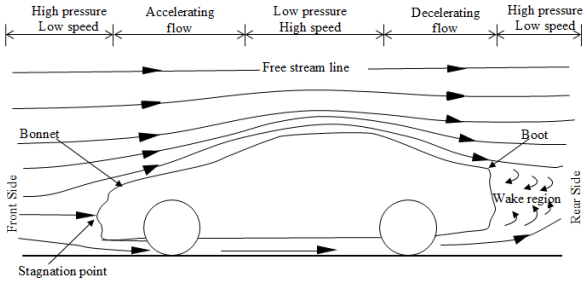

Fig. 1. Schematic of flow around a car.

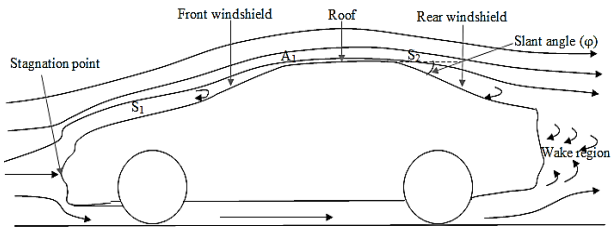

Fig. 2. Schematic of flow separation and attachment over the car surface.

components such as the engine exhaust. Among all these, flow over the surface of the car is significant to analyze, as it majorly contributes to the aerodynamic forces and moments acting on the car. When the car is moving, the flow region between the top surface of the vehicle to the outer streamline also known as the free streamline can be considered to create a venturi effect as shown in Fig. 1. This effect leads to various pressure regions along with the profile of the car body due to surface changes. If the speed of the vehicle increases, the pressure in the front of the car will increase, and that in the back will decrease (Wassen & Thiele, 2009).

Flow separation and wake regions take place at various locations on the car surface. The flow separation is witnessed in two locations on the car surface as shown in Fig. 2. The flow separation (*S1*) occurs between the bonnet and windshield due to the sudden change in the car profile and flow attachment (*A1*) happens near the front roof. The second flow separation (*S2*) happens near the rear windshield region due to a slant angle (φ) - the angle between the windshield and free streamline, and the separated flow leaves the car surface creating a wake region at the backside of the car (Peng et al., 2023). Such a flow phenomenon along with the varying pressure levels on the surface of the car creates the resisting force known as pressure drag contributing to 80% of the total drag of the car (Inchul & Hualei, 2010).

The drag of the passenger car is almost 80% of its total resistance when it moves above 20 m/s (70 *km/h*). At higher speeds, the drag impacts about half of the fuel utilization. The tractive power of the vehicle is directly proportional to the cubic velocity of the vehicle. The connection between fuel consumption and coefficient of drag is (Himeno & Fujitani, 1993)

$$\frac{\Delta FC}{FC} = \eta \times \left(\frac{\Delta C_D}{C_D} + \frac{\Delta A_f}{A_f} + 3\frac{\Delta U}{U} \right) \tag{1}$$

Where are FC - fuel consumption, A_f - frontal area of the car, η - the property of driving a car (approximately 0.5 to 0.7 for highway speed), and U – car speed.

2. BASEBLEED DESIGN

The pressure drag contributes to around 80% of the total drag of a car (Browand, 2007). Hence, it is highly important to reduce the wake region, in the rear end of the car, that contributes to the pressure drag. Thus, a drag reduction method to eliminate this wake region must be either by delaying the flow separation and hence the reduction in the wake or by supplying high momentum

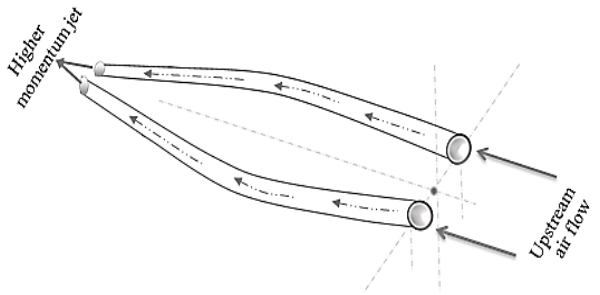

Fig. 3. Basebleed configuration proposed for drag reduction.

airflow to the wake region.

The Basebleed method is a fully aerodynamics-based technique adopted from rocket technology for thrust vectoring. In this method, two converging hollow tubes having a cross-sectional area of the front side greater than that of the rear side are configured as shown in Fig. 3.

The Inlet of the basebleed tube sucks the upstream air in the front region of the car while moving and reduces the total pressure in that region. The air sucked in the tube gets accelerated, as the cross-sectional area of the tube gradually decreases, making it tapered towards downstream. Hence, a higher momentum jet comes out of the tubes that are focused on the center of the wake region. These higher momentum jets interact with each other where the conversion of kinetic energy to pressure energy takes place. This collided jet fills the wake region and energizes it. Thus, the total pressure in the rear end of the car gets increases. This reduction in pressure at the front and increase in pressure at the rear leads to the change in differential pressure that contributes to pressure drag and reduces it.

For this study, the basebleed configuration is chosen based on the size of the car. The detailed specification of the basebleed configuration for this study is given in Table 1.

The basebleed tubes can be installed under the floor of the car and it does not affect any internal parts of the car as shown in Fig. 4. For this study, the basebleed tube's cross-section was chosen as circular for better flow distribution.

A 3-Dimensional model and schematic of a hatchback car with basebleed are shown in Fig. 4. The basebleed inlet and outlet tubes are located at the same distance from the central axis of the car. The distance between the basebleed inlets at the front end of the car is denoted as B_f whereas the distance between basebleed outlets at the rear end is

Table 1 Various dimensions of basebleed configuration.

Specification	Dimension
Length of basebleed tube	412 mm
Diameter of the frontal cross-section of basebleed (Φ)	9 mm
Area of the frontal cross-section of basebleed	63.6 mm^2
Diameter of the rear cross-section of basebleed (Φ)	4 mm
Area of the rear cross-section of basebleed	12.56 mm^2
Total number of tubes	2 (Numbers)

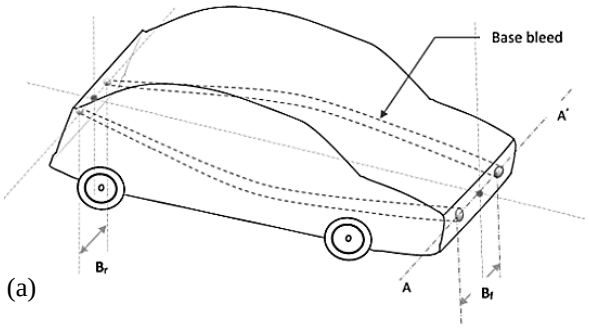

(a)

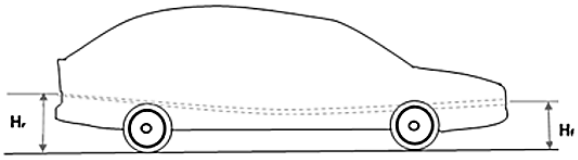

(b)

Fig. 4. Schematic of hatchback car with basebleed (a) isometric view (b) side view.

denoted as B_f. Likewise, the height of the basebleed centerline is located at the height H_f in the front end and H_r in the rear end. Since, the drag reduction method can be applied to vehicles of any size and the specifications of basebleed technique such as distance (B_f, B_r) and height (H_f, H_r) can be followed as the ratio in reference to the breadth and ground clearance of the vehicle, respectively. The ratios are defined as

- Distance ratio of B_f - Ratio of the distance between basebleed inlets and breadth of the car at the front side.
- Distance ratio of B_r - Ratio of the distance between basebleed outlets and breadth of the car at the rear side.
- Distance ratio of H_f - Ratio between the height of basebleed inlets from the ground and ground clearance at the front side.
- Distance ratio of H_r - Ratio between the height of basebleed outlets from the ground and ground clearance at the rear side.

Based on the previous experimental study (Sivaraj et al., 2018), the optimal position of the basebleed of the hatchback car model is fixed to analyse the numerical simulation in terms of distance and height ratios as B_f =0.7, B_r =0.2, H_f =3.5, H_r =4.5.

Table 2 Dimensions of hatchback car model followed for the numerical study

Specification	Dimension (mm)
Length (L)	402
Breadth (B)	176
Height (H)	156
Ground Clearance (G C)	16

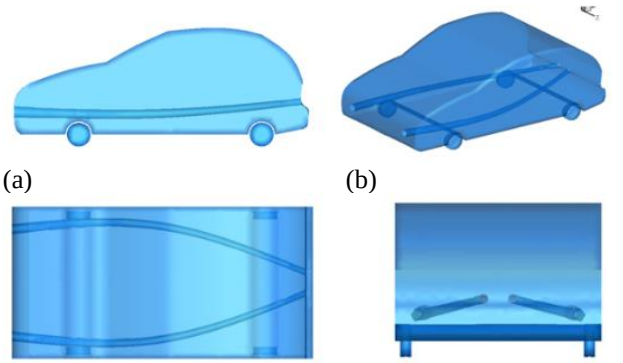

(a) (b)

(c) (d)

Fig. 5. Different views of hatchback car model with basebleed (a) side view, (b) isometric view, (c) bottom view, (d) back view.

3. NUMERICAL STUDY

In order to overcome the limitations of the experimental study such as the lack of a 3-dimensional flow picture, the numerical analysis of flow dynamics of the hatchback car model with and without basebleed technique using ANSYS-Fluent was done for the same flow conditions.

3.1 Geometry Construction

The hatchback car models with and without attachment of basebleed were chosen for computational studies. 1:10 scaled models followed for the previous experimental study were designed for the numerical study in CATIA V6. The dimensions of the car models are given in Table 2. Figure 5 shows three different views of the solid model of the hatchback car with a basebleed design. The length, height, and breadth axes of the car models were aligned with the x, y, and z axes of the computational domain.

The computational domain is created in a cuboid shape of 4000 mm × 2000 mm × 2000 mm (length (l) × height (h) × breadth (b)). The dimensions of the computational domain in length, height, and width are normalized with car length (L) such as 10L, 5L, and 5L respectively as shown in Fig 6. The computational domain surfaces are named inlet, outlet, ceiling wall, and road wall.

The car models are positioned at a distance of 3L of the car from the inlet of the computational domain where the 7L distance at the rear end will be significant enough for analysing the rear field flow. The car models were placed

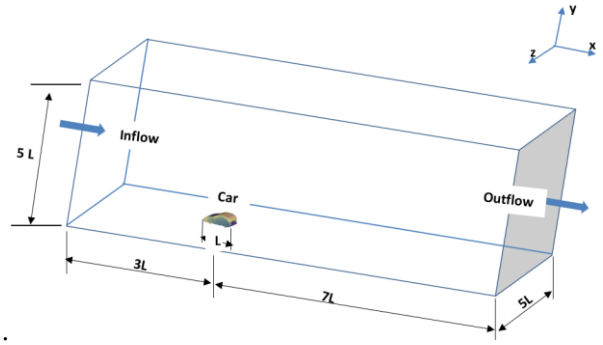

Fig. 6. Computational domain with dimension specifications.

at the road wall in the *y*-direction and the center point of breadth in the *z*-direction

3.2 Grid Generation

Grid for the numerical study in the defined computational domain was done using the inbuilt meshing module of ANSYS-Fluent 15.0. An unstructured tetrahedral mesh with prism layers near the hatchback car model was generated. The prism layer growth rate was set to 1.2 with a *Y*+ value of 30. The numerical simulation is studied using the k-ε turbulence model and analyzed the wake regions over the surface of the hatchback car model with and without basebleed. However, the basebleed is significantly not influencing the flow separation and attachment of flow fields on the boundary layer of the car surface. Hence, *Y*+ values are not affecting the overall result and the flexibility of *Y*+ values is maintained 30 to carry out the simulation process very smoothly (Connor et al., 2006). Near the car surface, the mesh was maintained as a fine structure, and towards the edges of the computational domain, the mesh tends to be coarsely structured (Wang et al., 2014).

The fine region near the car surface is shown in Fig. 7 whereas the mesh structure is clearly observed close to the car surface to capture the boundary layer. Four different mesh sizes were followed in order to complete the grid independence test before choosing the grid size for the numerical study. Four different mesh sizes with 3.21×10^6, 9.84×10^6, 1.82×10^7, and 2.91×10^7 cells named Mesh 1, Mesh 2, Mesh 3, and Mesh 4, respectively, were chosen to generate coarse to fine mesh. The basebleed method introduced in a car is especially to reduce the wake region at the rear side of the vehicle by adding energy to the flow. *k*-*ε* turbulence model was found to be better suitable for studying the wake regions and far from the boundaries. Hence, the *k*-*ε* turbulence model has opted and the hatchback car is subjected to the numerical simulation process ranging to 20 m/s to study the turbulence behavior with and without basebleed.

In the flow field over the surface of a car, flow separation and attachment are not affected by the implementation of the basebleed. Hence, this research is significantly not influenced by the boundary layer factor. However, the *k*-*ω* model is very efficient to predict the turbulence parameters which are very close to the boundary. The *SST* model is also an improved version of the *k*-*ω* model. Previous research indicates that the wake regions studied by the *k*-*ε* model are more accurate compared to other models (Connor et al., 2006). Hence *k*-*ε* turbulence model has opted for numerical simulation.

As drag was the main parameter of focus for the study, the C_D was obtained from simulations of different mesh sizes for comparison. C_D values for different mesh sizes have been plotted and shown in Fig. 8. From the Grid Independence Study (GIS), it can be found that the reduction in C_D was about 11% when the mesh was made finer (Mesh 4) from coarser (Mesh 1). Mesh 3 and Mesh4 despite a different number of cells in the computational volume results in the same C_D value of about 0.33. Hence, the coarser mesh (Mesh 3) with 18264412 cells was chosen for the numerical study to reduce the computational time (Renan & Francisco, 2015).

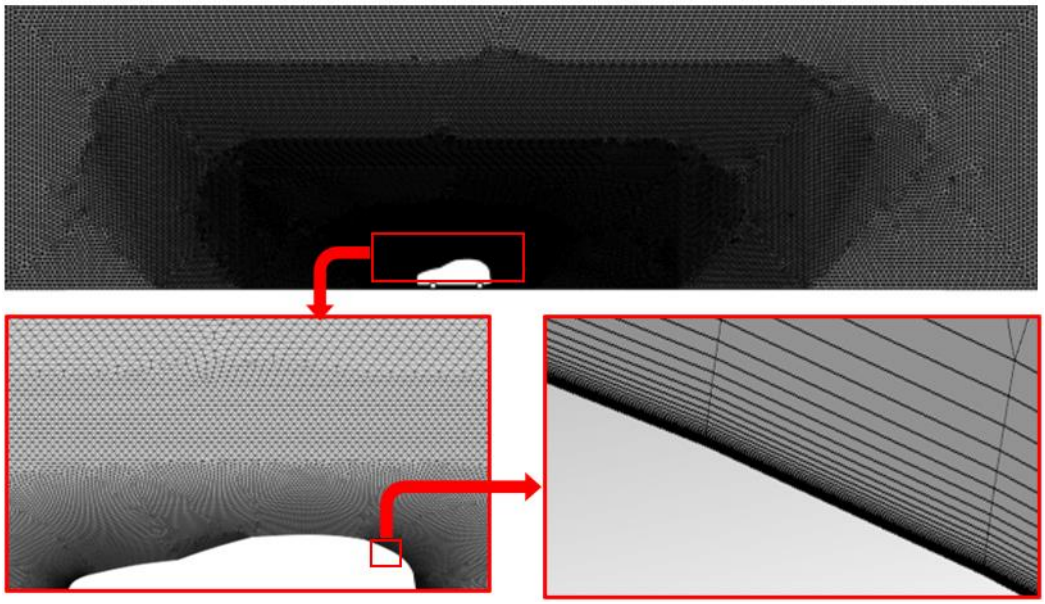

Fig. 7. Unstructured grid generated in the computational domain for numerical study.

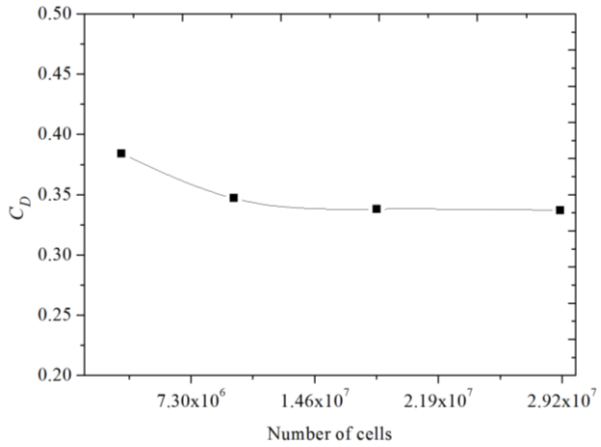

Fig. 8. C_D trend for various mesh sizes followed for grid independence study

3.3 Numerical Solver

Based on GIS, the fine mesh (mesh 3) with 18264412 elements was chosen for the numerical study using ANSYS Fluent 15. The boundary condition at the inlet was set to a steady flow velocity of 20 m/s whereas the outlet pressure was left the same as the operating pressure. Ceiling, road, sidewalls, and car surfaces were defined as wall boundaries for the simulations where the road was assumed as a moving wall. A computational study was done in a pressure-based solver using the *k-ε* turbulence model. The reliable *k-ε* turbulence model (Altaf et al., 2014; Andrew et al., 2009) was found to be better for boundary layer separation, flow attachment, wake formation, and turbulent flow. Turbulence intensity was set at 4% (Aleksander & Milan 2017, Giacomo et al., 2017) and the turbulent viscosity ratio was set to eight for the walls with no-slip conditions. The finite volume CFD code of the desired model was used to solve the following continuity and momentum equations (2) to (5) of the desired domain (Bert et al., 2023).

Continuity equation

$$\nabla \cdot (\rho \cdot U) = 0 \tag{2}$$

x-momentum equation

$$\nabla \cdot (\rho \cdot u \cdot U) = -\frac{\partial P}{\partial x} + \frac{\partial \tau_{xx}}{\partial x} + \frac{\partial \tau_{yx}}{\partial y} + \frac{\partial \tau_{zx}}{\partial z} + \rho f_x \tag{3}$$

y-momentum equation

$$\nabla \cdot (\rho \cdot v \cdot U) = -\frac{\partial P}{\partial y} + \frac{\partial \tau_{xy}}{\partial x} + \frac{\partial \tau_{yy}}{\partial y} + \frac{\partial \tau_{zy}}{\partial z} + \rho f_y \tag{4}$$

z-momentum equation

$$\nabla \cdot (\rho \cdot w \cdot U) = -\frac{\partial P}{\partial z} + \frac{\partial \tau_{xz}}{\partial x} + \frac{\partial \tau_{yz}}{\partial y} + \frac{\partial \tau_{zz}}{\partial z} + \rho f_z \tag{5}$$

Convergence of the governing equation was achieved in the order of 10^{-6}. During post-processing of the numerical results, flow visualization was done to understand the detailed flow profiles at various cross sections as well as in the 3D domain. Velocity profiles, lift, and drag was obtained based on the numerical simulation to compare previous experimental study. Additionally, Turbulent Kinetic Energy (TKE) was calculated for the simulated condition.

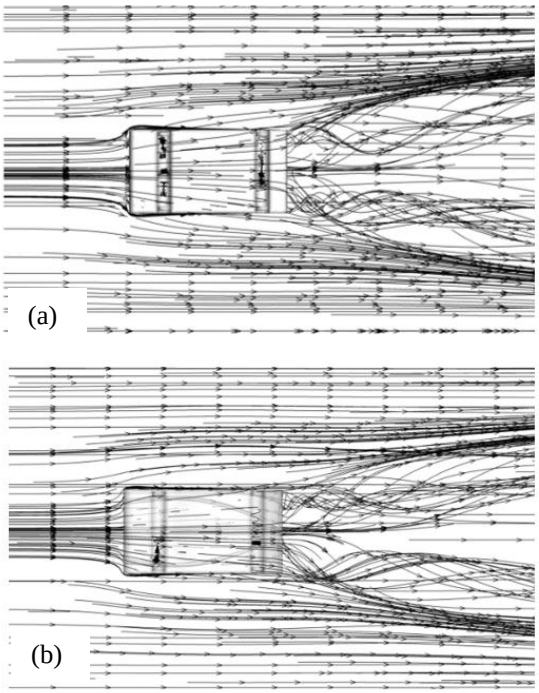

Fig. 9. Streamlines pattern over a hatchback car model. (a) without basebleed (b) with basebleed.

4. Results and Discussion

The 3-Dimensional flow details of flow around the hatchback car model with basebleed design were obtained from numerical results. Figure 9 a shows the streamlines over the hatchback car model without basebleed. Upstream flow with higher momentum withstands the front region of the hatchback car model without flow separation until the end of the bonnet on the side surfaces. In the rear surface at the end, the flow leaves the car surface as a shear layer curls into vortex filaments at both edges having straight streamlines in between. Wherein, Fig. 9 b shows the streamline pattern over a hatchback car model with basebleed. The suction of higher momentum upstream flow into the basebleed tubes lead to the accumulation of higher momentum flow towards the front region resulting in earlier flow separation right at the edges of the bonnet. However, a small number of flow slides over the side surfaces of the car model till the end. This flow merges with the vortex filaments at the rear end edges. Due to the supply of higher momentum, the vortex filaments in the rear end gain strength with a reduction in the wake region between them. At the same time, the collision of basebleed jets increases the pressure between those vortex filaments and reduces the wake. This can be seen in the velocity fields and pressure fields shown in Figs 10 and 12, respectively.

Figure 10 shows the mid-plane velocity distribution of flow over the hatchback car model with and without basebleed. A comparison between Fig. 9 a and b reveals that the basebleed, though installed near the bottom surface, has the ability to influence the overall flow pattern around the hatchback car model. In the front region, a higher area of high velocity is observed for the hatchback car model with basebleed. Higher velocity regions were

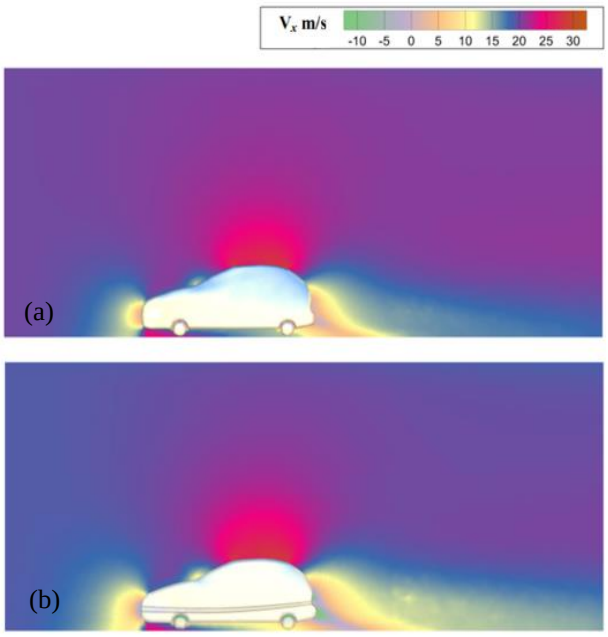

Fig. 10. Mid-plane velocity distribution of flow over the hatchback car model. (a)without basebleed (b) with basebleed

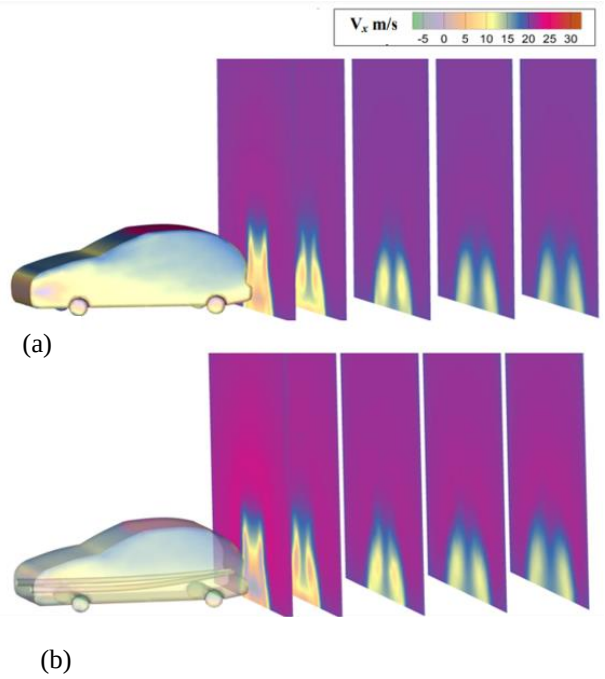

Fig. 11. Rear end flow field at various planes along the longitudinal axis of the hatchback car model. (a) without basebleed (b) with basebleed

observed at the bonnet and top surface, whereas lower velocity was observed at the bottom surface of the hatchback car model with basebleed. It can be inferred that the flow velocity at the front side is minimum due to the direct collision of the airflow at the front bonnet and the maximum velocity is reached near the roof of the car. This certainly shows the alteration of the flow field around the hatchback car model after the installation of the basebleed. Such an alteration will lead to a change in the overall drag of the hatchback car model.

In the rear end region, an increase in higher velocity regions was observed after the installation of the basebleed. Additionally, the immediate downstream of the rear end shows reduced velocity which leads to increased pressure in the hatchback car with basebleed. This indicates that the basebleed not only contributes to the pressure in the wake region but also the momentum of vortex filaments created from the horizontal edges of the rear end of the hatchback car model. This phenomenon is clearly shown in Fig. 11 where the rear end flow field at various planes along the longitudinal axis. However, this effect is prominently seen only in the immediate downstream up to two planes.

Pressure distribution in the rear end of the hatchback car model with and without basebleed is shown as midplane coefficient of pressure (C_P) distribution in Fig. 12. Figure 12b shows the increase in the high-pressure region immediately downstream of the hatchback model after the installation of the basebleed. The high-pressure region also extends longitudinally for a higher distance when compared to the hatchback car model without basebleed. This is clearly shown at various planes downstream of the hatchback car model in the longitudinal direction as shown in Fig. 13.

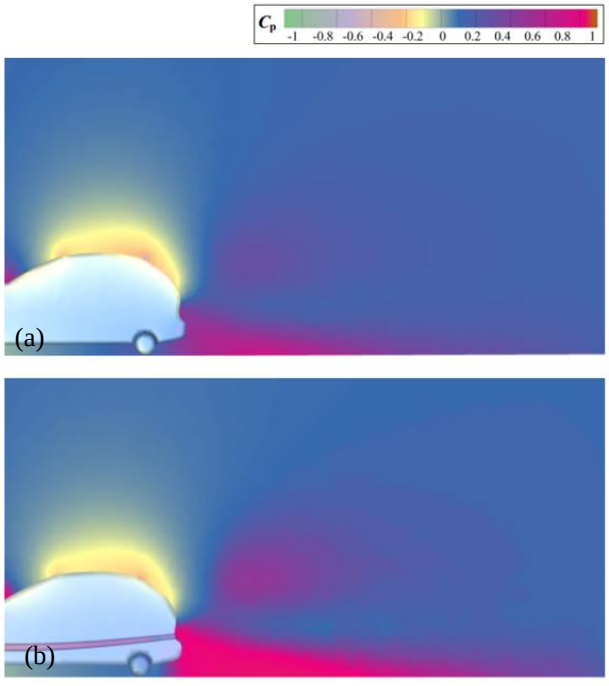

Fig. 12. C_P distribution at mid-plane of the hatchback car model. (a) without basebleed (b) with basebleed

Similar to the velocity distribution, the pressure distribution also shows the prominent change in the immediate downstream of the hatchback car model with basebleed. The coefficient of pressure (C_P) distribution over the hatchback car model with and without basebleed given in Fig. 14 shows the increased pressure in the rear end surface of the hatchback car model with basebleed.

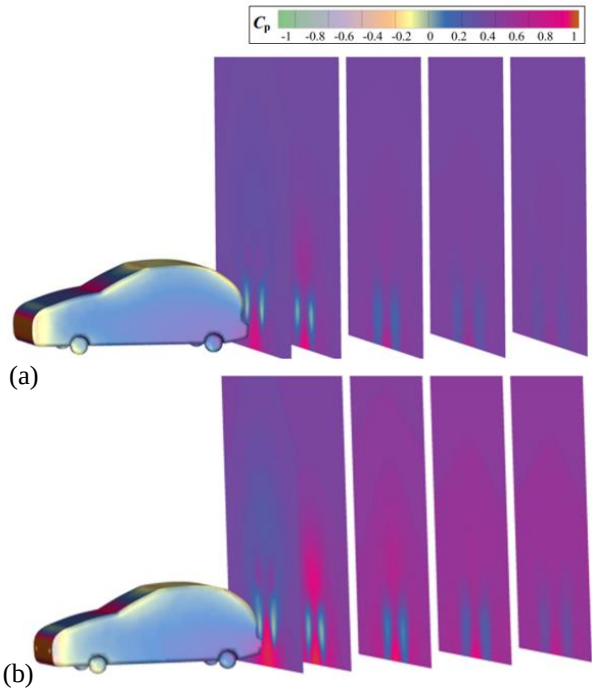

Fig. 13. Rear end C_P distribution at various places along the longitudinal axis of the hatchback car model. (a) without basebleed (b) with basebleed

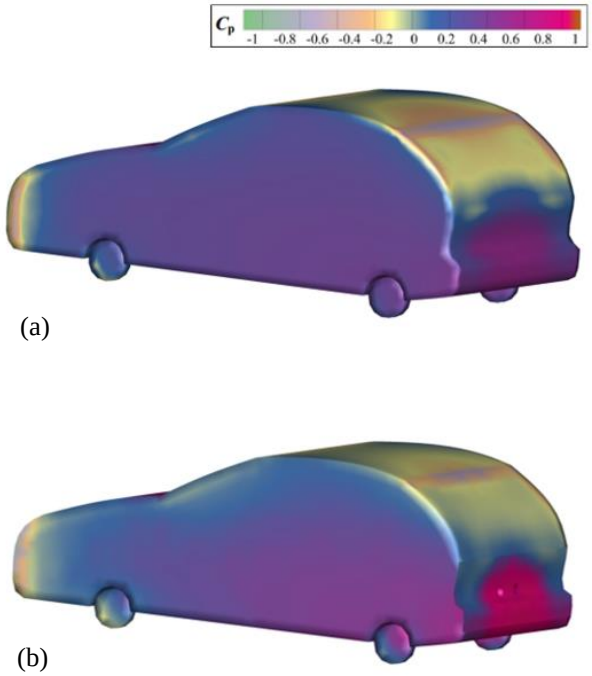

Fig. 14. C_P distribution over the hatchback car model. (a)without basebleed (b) with basebleed

this increased pressure effectively contributes to the reduction of drag.

The coefficient of pressure (C_P) on Hatchback cars without basebleed and with basebleed is shown in Fig. 15. To understand the clarity of results, the co-efficient of pressure (C_P) values are considered for 40 profile points at the mid-plane of the car surface. The comparative study

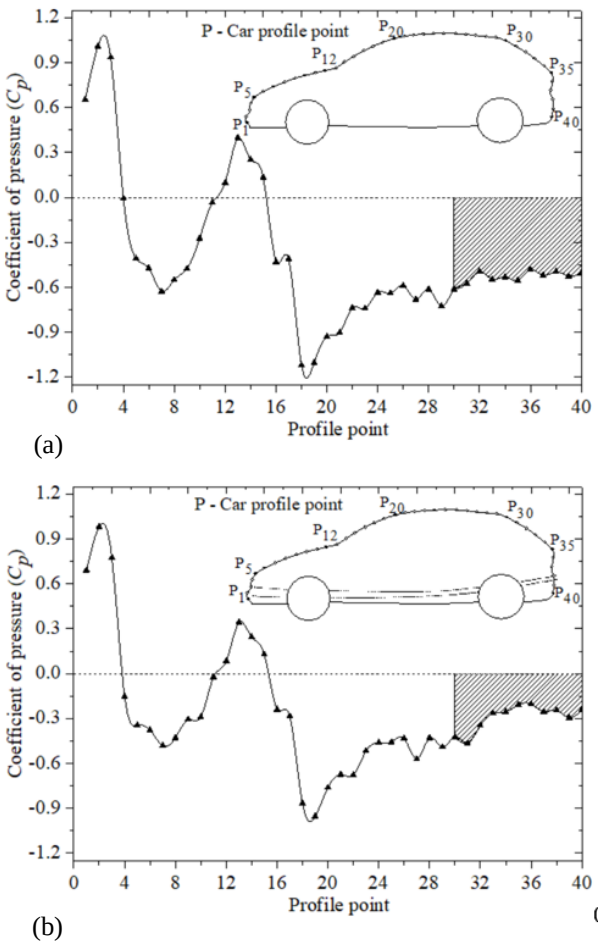

Fig. 15. C_P distribution on hatchback car model (a) without and (b) with basebleed.

shown in Fig. 15 (a) & (b) yields the overall trends for the coefficient of pressure (C_P) distribution is similar for both with and without basebleed whereas the magnitude of pressure changes at the rear end of the hatchback car. The profile points between 29 to 40 are located in the rear end region under the C_P curve and is hatched for both hatchback car with and without basebleed. Figure 15 shows the summation of the magnitude of C_P for the hatchback car model with basebleed is noticeably lower than that of the hatchback car model without basebleed at the rear side. Hence, it is clear that the pressure is additionally provided in the wake region of the hatchback car model with the help of basebleed. High momentum air flow emanated at the basebleed tubes in the rear end collide and hence the kinetic energy is converted to pressure energy. Further, it was noticed in the computational simulation process that the centre line of mean C_P for the hatchback car model without basebleed ranges 0.239, - 0.582, and - 0.624 at the front side, top surface, and rear side respectively whereas the coefficient of drag (C_D) is obtained as 0.338. However, the centre line mean coefficient of pressure (C_P) for the car model with basebleed is 0.217 at the front side, - 0.569 at the top surface, and - 0.591 at the rear side, and the coefficient of drag (C_D) reached 0.313.

Turbulent intensity, a conventional way of quantifying the momentum loss in a flow field was followed to

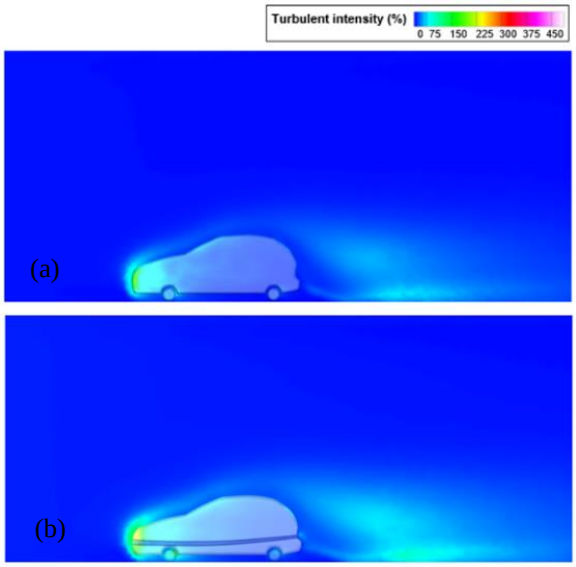

Fig. 16. Turbulent intensity at the center plane of the hatchback car model. (a) without basebleed (b) with basebleed.

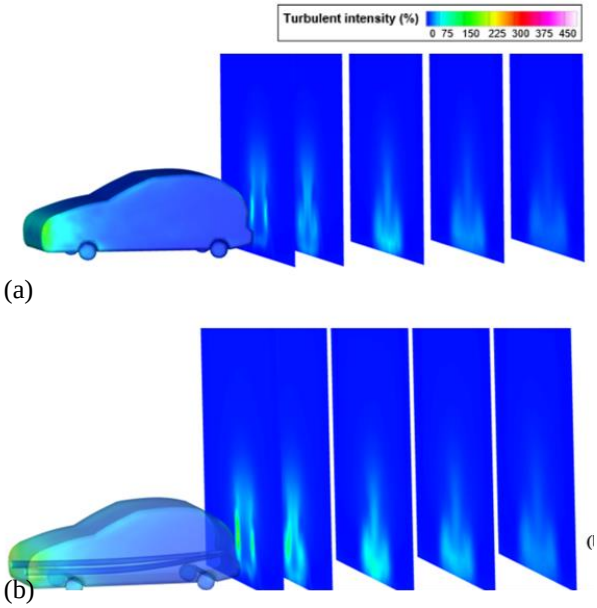

Fig. 17. Turbulent intensity at various planes along the longitudinal axis of the hatchback car model. (a)without basebleed (b) with basebleed.

understand the drag reduction in this study. Figures 16 & 17 show the turbulent intensity over the hatchback car model with and without basebleed. The variations of turbulent intensity of the car models are evident that the pressure is additionally provided in the wake region at the rear side of the car with the help of basebleed. High momentum air flow coming out of basebleed tubes in the rear end collided and hence the kinetic energy is converted to pressure energy.

The benefit of the basebleed attached in the hatchback car is clearly explicated at various yaw angles (ψ) and shown in Figs 18 to 20. When the basebleed is attached to the car model the drag and side force coefficients (C_D and C_S) were reduced at all the yaw angles followed for this study, compared to the hatchback car model without basebleed. Figure 18 shows that the C_L value maintains negligible variation for all yaw angles (ψ). Thus, it is clear from Figs 18 and 19 that the lift and side forces that cause instability to the car are maintained constant and reduced, respectively, with basebleed attachment in the hatchback car model. Hence, the stability of the car is not affected by installing the basebleed.

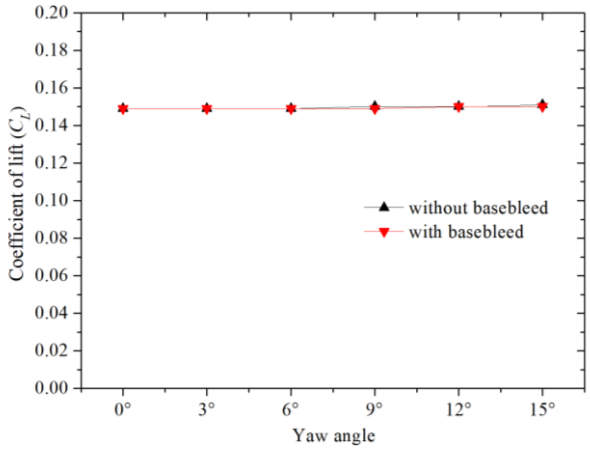

Fig. 18. Comparison of C_L on hatchback car The model with and without basebleed for various yaw angle.

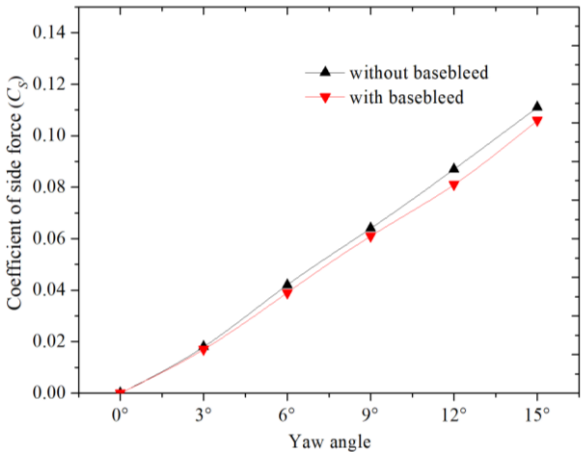

Fig. 19. Comparison of C_S for hatchback car model with and without basebleed for various yaw angle.

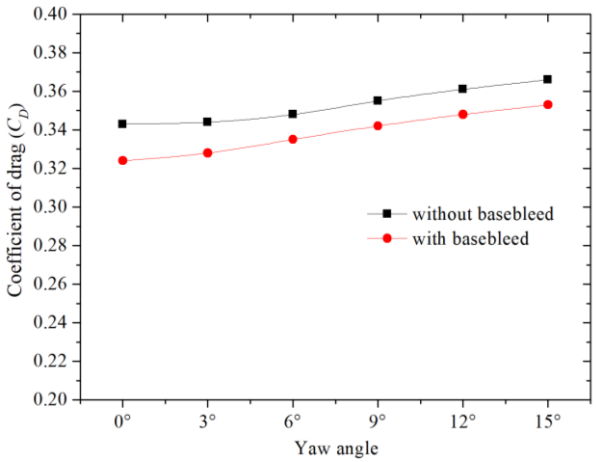

Fig. 20. Comparison of C_D for hatchback car model with and without basebleed for various yaw angle.

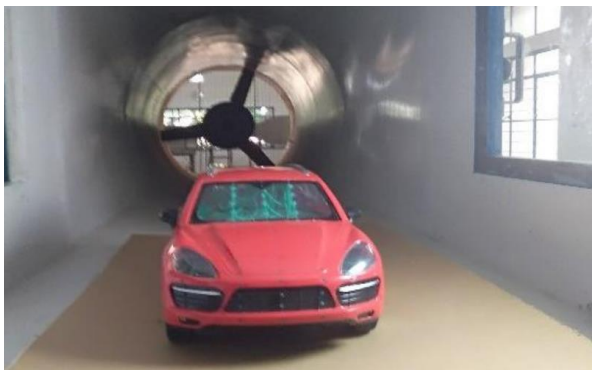

Fig. 21. Experimental setup.

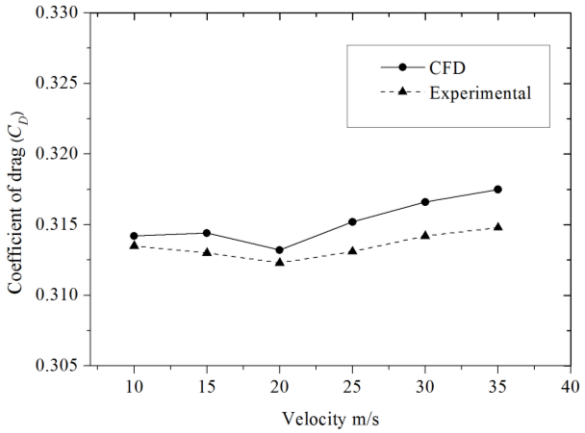

Fig. 22. Comparison of C_D obtained from experimental and numerical studies for hatchback car model with basebleed.

It is found in Fig. 20 that the C_D is reduced by 6 % at the yaw angle of the car model $\psi = 0°$. After that, the C_D is further reduced up to 4 % at $\psi = 6°$ and the same is maintained for the remaining angles. Such a large decrease in C_D is a result of a modified flow pattern at the rear side due to the installation of the basebleed. The coefficient of Drag (C_D) reduction is maintain the same reduction rate for higher yaw angles up to 15°.

In order to validate the computational results, a comparative study was carried out with existing computational and previous experimental results (Sivaraj et al., 2018). The existing experimental results were obtained using an open circuit subsonic wind tunnel with adequate setup of real road conditions for a 1:10 scaled hatchback car model with basebleed as shown in the Fig. 21. The surface pressure of hatchback car models was measured from the pressure port at a constant flow condition inside the test section. Based on the surface pressure measurements, the coefficient of pressure (C_P) and coefficient of drag (C_D) are obtained for various velocities ranges 10 m/s to 35 m/s. The position of car profile points in the numerical result is replicated from the pressure port positions. The coefficient of drag (C_D) of the hatchback car model with basebleed obtained from the numerical studies of the current research and previous experimental results are given in Fig. 22. However, only a notably small variation in (C_D) with velocity was observed.

The results show the percentage of error in the aerodynamic coefficient of drag (C_D) in experimental tests and computational study ranges to a minimum of 0.23 % and a maximum of 0.35 %. The error percentage of the coefficient of drag (C_D) obtained from the experimental test and numerical studies is less than 1%. Hence the numerical approach in this research satisfies the calculation requirements.

As mentioned in section 1.1, the reduction in drag can be related to the fuel consumption of the vehicle. Based on equation (1) the fuel consumption of the vehicle will reduce by 11% if the ratio of reduction in C_D and C_D (ΔC_D/ C_D) is 0.22 as given by Browand (2007). From this study, the ratio of reduction in C_D and C_D (ΔC_D/ C_D) after the installation of basebleed in a hatchback car model is found to be C_D 0.09. This implies, based on equation (1), that the reduction in fuel consumption after the installation of basebleed turns out to be around 4.3%.

Since the basebleed method of drag reduction is done through an additional mechanism to a hatchback car. The alteration in the rear flow field due to the high-momentum air is inevitable. This rear-end flow field will alter the upstream flow of the following car and hence it affects the drag of the following car. According to Simon and Gioacchino (2008), the aerodynamic analysis of the interference effect of space between two vehicles shows that a leading car doesn't affect the drag force on the rear car until the spacing between the cars reaches X/L = 0.4. The vehicle goes more than 70 *km/h* on the highway whereas none of the cars comes closer to the spacing X/L = 0.4. Hence basebleed attached to a car not impacting the other following cars in any aspect.

5. CONCLUSION

Investigation on the hatchback car model integrated with and without the basebleed method was studied using a numerical simulation process. From this research study, the following conclusions are made. The flow patterns around the hatchback car model with basebleed clearly notified the high momentum of airflow emanating from basebleed tubes and collided at the rear end of the car. The velocity and pressure distributions around the car models were observed from the contour of the coefficient of pressure and velocity. It was noted that pressure increased at the rear side and that influenced the reduction of the wake regions in the car. The variations of turbulent intensity of the car models are evident in the reduction of drag by increasing the pressure at the rear side of the car with the help of basebleed. The research recommended that the hatchback car model installed with basebleed arrived 6% of reduction in coefficient of drag (C_D) and suggested implementing it for other rear-end shape car models such as sedan, squareback, and fastback car models. Further, the numerical results of the coefficient of lift (C_L) and coefficient of side force (C_S) for the varying yaw angle (ψ) analysis prove that the stability of the car was not affected while using this basebleed method. The main objective of this research was achieved, hence the reduction in fuel consumption of the hatchback car model after the installation of basebleed is attained at 4.33%.

ACKNOWLEDGEMENTS

The authors would like to thank the Subsonic Airflow Testing Facility, Research Park, Bannari Amman Institute of Technology for their support during the computational analysis.

CONFLICT OF INTEREST

The authors have no conflict of interest to disclose in this research work.

AUTHORS CONTRIBUTION

G Sivaraj: Developed conceptualization, methodology, and validation; K. M Parammasivam: Performed writing - Oral draft preparation; M. S Prasath: Performed writing - Designing and Analsis; D. Lakshmanan: Performed writing - reviewing and editing.

REFERENCES

Aleksander, G., & Milan, B. (2017). Vehicle aerodynamic stability analysis under high crosswinds, *Strojniski vestnik. Journal of Mechanical Engineering*, 63(3), 191-200. https://doi.org/10.5545/sv-jme.2016.4095

Altaf, A., Ashraf, A. O., & Waqar, A. (2014). Passive Drag Reduction of Square Back Road Vehicles. *Journal of Wind Engineering and Industrial Aerodynamics*, 134, 30-43. https://doi.org/10.1016/j.jweia.2014.08.006

Andrew, D. L., Johnathan, J. K., & Matthew, S. (2009). *An Investigation into Unsteady Base Bleed for Drag Reduction in Bluff Two-Box SUV's*. European Automotive Simulation Conference, Munich, Germany.

Bert, B., Stefanie, G., Fabio, M., & Thijs, V. D. (2023), Impact of a nearby car on the drag of a cyclist. *Journal of Wind Engineering & Industrial Aerodynamics*, 234(1), 353 -359. https://doi.org/10.1016/j.jweia.2023.105353

Browand, F. (2007). *The Aerodynamics of Heavy Vehicles II: Trucks, Buses and Trains*. Global Climate and Energy Project on Advanced Transportation, Stanford University.

Connor, C., Kharazi, A., Walter, J., & Martindale, B. (2006). Comparison of wind tunnel configurations for testing closed-wheel race cars: a CFD study. *SAE Technical Paper*, 2006-01-3620. https://doi.org/10.4271/2006-01-3620

Giacomo, R., Christophe, S., Valeri, F., Jacques, B., & Fabien, H. (2017). Aerodynamic performances of rounded fastback vehicle. *Journal of Automobile Engineering*, 231, 1211–1221. https://doi.org/10.1177/0954407016681684

Gregoire, F., Laurent, K., Larbi, L., & Patrick, G. (2011). Bluff-body drag reduction using a deflector. *Experimental Fluids*, 50, 385-395. https://doi.org/10.1007/s00348-010-0937-6

Himeno, R., & Fujitani, K. (1993). Numerical analysis and visualization of flow in automobile aerodynamics development. *Journal of Wind Engineering and Industrial Aerodynamics*, 46, 785-790. https://doi.org/10.1016/0167-6105(93)90354-Q

Hucho, W., & Sovran, G. (1993). Aerodynamics of road vehicles. *Annual Review of Fluid Mechanics*, 25(1), 485-537. https://doi.org/10.1146/annurev.fl.25.010193.002413

Inchul, K., & Hualei, C. (2010). Reduction of aerodynamic forces on a minivan by a pair of vortex generators of a pocket Type. *International Journal of Vehicle Design*, 53 (4), 300–316. http://dx.doi.org/10.1504/IJVD.2010.034103

Kang, S. O., Jun, S. O., Park, H. I., Song, K. S., Kee, J. D., Kim, K. H. & Lee, D. H. (2012). Actively translating a rear diffuser device for the aerodynamic drag reduction of a passenger car. *International Journal of Automotive Technology*, 13(4) 583-592. https://doi.org/10.1007/s12239-012-0056-x

Kounenis, C., Bonitz, S., Ljungskog, E. & Sims Williams, D. (2016). Investigations of the Rear-End Flow Structures on a Sedan Car. *SAE Technical Paper*, 2016-01-1606. https://doi.org/10.4271/2016-01-1606

Mahmoud, K., Hicham, E. H., Fabien, H., & Hassan, P. (2012). Some innovative concepts for car drag reduction: A parametric analysis of aerodynamic forces on a simplified body. *Journal of Wind Engineering and Industrial Aerodynamics*, 108, 36-47. https://doi.org/10.1016/j.jweia.2012.03.019

Marklund, J., Lofdahl, L., Danielsson, H. & Olsson, G. (2013). Performance of an automotive under-body diffuser applied to a sedan and a wagon vehicle. *SAE International Journal of Passenger Cars – Mechanical System*, 6(1) 293-307. https://doi.org/10.4271/2013-01-0952

Matthew, W., & Simon, W. (2014). Aerodynamic Structure and Development of Formula 1 Racing Car Wakes. SAE Int. J. Passeng. Cars - Mech. Syst., 7(3),1096-1105. https://doi.org/10.4271/2014-01-0600

Peng, F., Yan, F., Yin, B. J., & Liang, J. N. (2023). Experimental study on wake characteristics of secondary grooved cylinders with different depths. *Journal of Applied Fluid Mechanics*, 16(5), 1057-1073. https://doi.org/10.47176/jafm.16.05.1592

Rakibul, H. S. M., Toukir, I., Mohammad, A., & Md Quamrul, I. (2014). *Numerical study on aerodynamic drag reduction of racing cars*. 10th International Conference on Mechanical Engineering, ICME 2013, Department of Mechanical Engineering, Bangladesh University of Engineering and Technology, Dhaka.

Renan, S., & Francisco, S. (2015). *Proposal of an aerodynamic concept for drag reduction of fastback car models*. SAE Technical Paper Series, 2015-36-

0523. https://doi.org/10.13140/2.1.3101.7762

Siddiqui, N. A., & Chaab, M. A. (2021). A simple passive device for the drag reduction of an ahmed body. *Journal of Applied Fluid Mechanics*, 14(1), 147-164. https://doi.org/10.47176/jafm.14.01.31791

Simon, W., & Gioacchino, V. (2008). The effect of vehicle spacing on the aerodynamics of a representative car shape. *Journal of Wind Engineering and Industrial Aerodynamics*, 96, 1232-1239. https://doi.org/10.1016/j.jweia.2007.06.042

Sivaraj, G., Parammasivam, K. M., Suganya, G. (2018). Reduction of aerodynamic drag force for reducing fuel consumption in road vehicle using basebleed. *Journal of Applied Fluid Mechanics*, 11(6), 1489-1495. http://dx.doi.org/10.29252/jafm.11.06.29115

Wang, Y., Xin, Y., Gu, Zh., Wang, Sh., Deng, Y., & Yang, X. (2014). Numerical and experimental investigations on the aerodynamic characteristic of three typical passenger vehicles. *Journal of Applied Fluid Mechanics*, 7(4), 659-671. https://doi.org/10.36884/jafm.7.04.21460

Wassen, E., & Thiele, F. (2009). *Road vehicle drag reduction by combined steady blowing and suction.* AIAA Fluid Dynamics Conference, San Antonio, Texas.

Yang, X., Hu, Y., Gong, Z., Jian, J., & Liu, Z. (2022). Numerical study of combined drag reduction bases on vortex generators and riblets for the ahmed body using iddes methodology. *Journal of Applied Fluid Mechanics*, 15(1), 193-207. https://doi.org/10.47176/jafm.15.01.32832